The Meteoritical Society

Meteoritics & Planetary Science 42, Nr 3, 357–372 (2007)
Abstract available online at http://meteoritics.org

Thermal alteration of hydrated minerals during hypervelocity capture to silica aerogel at the flyby speed of Stardust

Takaaki NOGUCHI[1*], Tomoki NAKAMURA[2], Kyoko OKUDAIRA[3, 4], Hajime YANO[4], Seiji SUGITA[5], and Mark J. BURCHELL[6]

[1]Department of Materials and Biological Sciences, Ibaraki University, 2-1-1 Bunkyo, Mito 310-8512, Japan
[2]Department of Earth and Planetary Sciences, Faculty of Science, Kyushu University, 6-10-1 Hakozaki, Fukuoka 812-8512, Japan
[3]Graduate University of Advanced Studies (Sokendai), 3-1-1 Yoshinodai, Sagamihara 229-8510, Japan
[4]Institute of Space and Astronautical Science/Japan Aerospace Exploration Agency, 3-1-1 Yoshinodai, Sagamihara 229-8510, Japan
[5]Graduate School of Frontier Sciences, University of Tokyo, 5-1-5 Kashiwanoha, Kashiwa 277-8583, Japan
[6]School of Physical Sciences, University of Kent, Canterbury, Kent CT2 7NH, UK
[*]Corresponding author. E-mail: tngc@mx.ibaraki.ac.jp

(Received 11 January 2006; revision accepted 12 December 2006)

Abstract–Outside the Earth's atmosphere, silica aerogel is one of the best materials to capture fine-grained extraterrestrial particles in impacts at hypervelocities. Because silica aerogel is a superior insulator, captured grains are inevitably influenced by frictional heat. Therefore, we performed laboratory simulations of hypervelocity capture by using light-gas guns to impact into aerogels fine-grained powders of serpentine, cronstedtite, and Murchison CM2 meteorite. The samples were shot at >6 km s^{-1} similar to the flyby speed at comet P/Wild-2 in the Stardust mission. We investigated mineralogical changes of each captured particle by using synchrotron radiation X-ray diffraction (SR-XRD), transmission electron microscope (TEM), and field emission scanning electron microscope (FE-SEM). SR-XRD of each grain showed that the majority of the bulk grains keep their original mineralogy. In particular, SR-XRD and TEM investigations clearly exemplified the presence of tochilinite whose decomposition temperature is about 300 °C in the interior of the captured Murchison powder. However, TEM study of these grains also revealed that all the samples experienced melting and vesiculation on the surface. The cronstedtite and the Murchison meteorite powder show remarkable fracturing, disaggregation, melting, and vesiculation. Steep thermal gradients, about 2500 °C/μm were estimated near the surface of the grains (<2 μm thick) by TEM observation. Our data suggests that the interior of >4 μm across residual grains containing abundant materials that inhibit temperature rise would have not experienced >300 °C at the center.

INTRODUCTION

Silica aerogel is an ultralow density SiO_2 gel. It has been used to capture micrometeoroids on manmade satellites in low Earth orbit (LEO) (e.g., EuReCa [Burchell et al. 1999], Euro-MIR95 [Hörz et al. 2000], and SM/MPAC and SEED on the International Space Station [ISS] [Neish et al. 2005; Burchell et al. 2006]) to collect micrometeoroids and space debris, and on the Stardust spacecraft to collect cometary dust that emitted from 81P/Wild-2 comet (e.g., Brownlee et al. 2004; Zolensky et al. 2006). Hörz et al. (2000) have successfully recovered some micrometeoroids containing olivine, augite, diopside, troilite, chromite/magnetite, and helcynite from the aerogel mounted on the orbital debris collector (ODC) on the Mir Space Station. Zolensky et al. (2006) have also recovered cometary dust originating from 81P/Wild-2. However, there are few studies that focused on what happens during capturing process (e.g., Barrett et al. 1992; Burchell et al. 2006). Because silica aerogel is a high-performance insulator with a low thermal conductance (Hunt et al. 1991), it is difficult to release frictional heat from silica aerogel during capture of fine-grained projectiles. Therefore, it is important to determine the effect of frictional heat during capture. Accordingly, we have been using fine-grained minerals that have low decomposition temperatures and fine-grained fragments of Murchison CM chondrite. We used this meteorite not because its mineralogy is thought to be similar to the mineralogy of cometary dust, but because it contains minerals with low decomposition temperatures (Okudaira et al. 2002, 2003, 2004). In these earlier studies, we found that

antigorite and cronstedtite were melted, vesiculated, and mixed with surrounding aerogel during capture only on their surfaces, although cronstedtite experienced more severe melting than antigorite when both were shot at 3–4 km s^{-1}.

In this paper, we report detailed mineralogical investigation of captured particles shot at >6 km s^{-1}, which is the flyby speed of the Stardust spacecraft at comet Wild-2 (Brownlee et al. 2004). We used serpentine group minerals and Murchison meteorites as "thermosensors" with different sensitivities. However, the problem of whether or not phyllosilicates themselves exist in cometary dust is not resolved even today. We think that our results are useful in understanding mineralogical changes in phyllosilicates during hypervelocity capture in aerogel even if cometary dust contains phyllosilicates other than serpentine. We also have to consider the possibility that cometary dust contains phyllosilicates. For example, based on the study of interplanetary dust particles (IDPs), Rietmeijer (2004) argued that CI-like materials could come from comets. More recently, Lisse et al. (2006) reported that about 8% of silicates in dust generated by the Deep Impact spacecraft are occupied by phyllosilicates in 9P/Tempel-1. Their IR spectral data fit that of Na-bearing nontronite rather than those of saponite and serpentine, although such interpretations are treated with caution by some. In general, our results give a useful guide to selecting residual grains that are suitable for the mineralogical and chemical analyses of cometary dust captured by Stardust as well as those of micrometeoroids captured in low Earth orbits.

EXPERIMENTAL PROCEDURES

Powdered (average diameter about 150 μm) serpentine, cronstedtite, and Murchison meteorite were used as projectiles in this work. The powders were placed in sabots and shot by two-stage light-gas gun at Kent University. They were shot at normal incidence to the surface of aerogel. Details of the experimental conditions of the two-stage light-gas guns have been described in Okudaira et al. (2003, 2004). The density of silica aerogel used in this study is 0.03 g/cm^3. After detailed observation of tracks in aerogel (results will be presented elsewhere), captured particles were extracted from aerogel by hand under a stereomicroscope in a clean bench (class 100) in the clean room (class 1000) at Ibaraki University. All extracted particles used in this study are terminal particles that were found at the ends of tracks. In our experiments, particles that were observed along the tracks were too small to extract from the silica aerogel by our method. To characterize bulk mineralogy of the individual particles, we utilized synchrotron radiation X-rays at beam line 3A of the Photon Factory Institute of Material Science, High-Energy Accelerator Research Organization, Tsukuba, Japan. A particle sample was mounted on a thin glass fiber 5 μm in diameter and exposed to synchrotron X-rays in a Gandolfi camera that gives a powder diffraction pattern of the particle according to the scheme shown in Nakamura et al. (2001). The X-rays were monochromated to 2.161 ± 0.001 Å and concentrated by mirrors to a position of the Gandolfi camera. The X-ray diffraction pattern was recorded on X-ray films and the resulting X-ray patterns were digitized by scanning the films with a flatbed scanner. The ultrahigh intensity and well-monochromated synchrotron X-rays allowed us to obtain a clear X-ray powder diffraction pattern of each small particle with short exposure of 30–60 min.

After synchrotron radiation X-ray diffraction (SR-XRD), the particles were embedded in epoxy resin and ultramicrotomed into 70 nm ultrathin sections by using Leica-Reichert Supernova Ultramicrotome at Ibaraki University. The ultrathin sections were investigated by JEOL JEM-2000 FX transmission electron microscope (TEM) equipped with EDAX DX4 energy dispersive spectrometer (EDS) at Ibaraki University for detailed textural observation and chemical composition analysis of constituting materials in the sections. Because minerals in the samples were quite susceptible to changing their chemical compositions and to becoming amorphous during analysis by EDS, a liquid-nitrogen-cooled double-tilt analytical sample stage Gatan model 667 was used to prevent compositional changes during EDS analysis. A 100 to 200 nm beam was used for the analysis of anhydrous silicates. The beam diameter was changed from 300 to 500 nm for intact and partially decomposed serpentine, cronstedtite, tochilinite, and glass to minimize compositional change even using the liquid-nitrogen-cooled sample stage. Quantitative analysis was based on the Cliff-Lorimer thin film approximation. Experimental k-factors were obtained from many mineral standards. We also used the potted butts (remainder epoxy rods after ultramicrotomy) to observe overall cross sections of each sample by using JSM-6700 field emission scanning electron microscope (FE-SEM) at JEOL Co., Ltd.

RESULTS

Synchrotron Radiation X-ray Diffraction of Captured Particles

Figure 1 shows synchrotron radiation X-ray diffraction charts of captured projectiles of serpentine, cronstedtite, and Murchison meteorite shot at >6 km/s and recovered from silica aerogel as well as those taken before the shots. Sample names and experimental conditions are shown in Table 1. Diffraction peaks in all captured samples are almost identical to the peaks from before the shots except for cronstedtite. Although some diffraction peaks disappeared in the captured cronstedtite when compared with that from before the shot, it is not clear whether this difference is inherent or not (Figs. 1c and 1d). These data do, however, show that abundant secondary minerals were not formed during capture in these

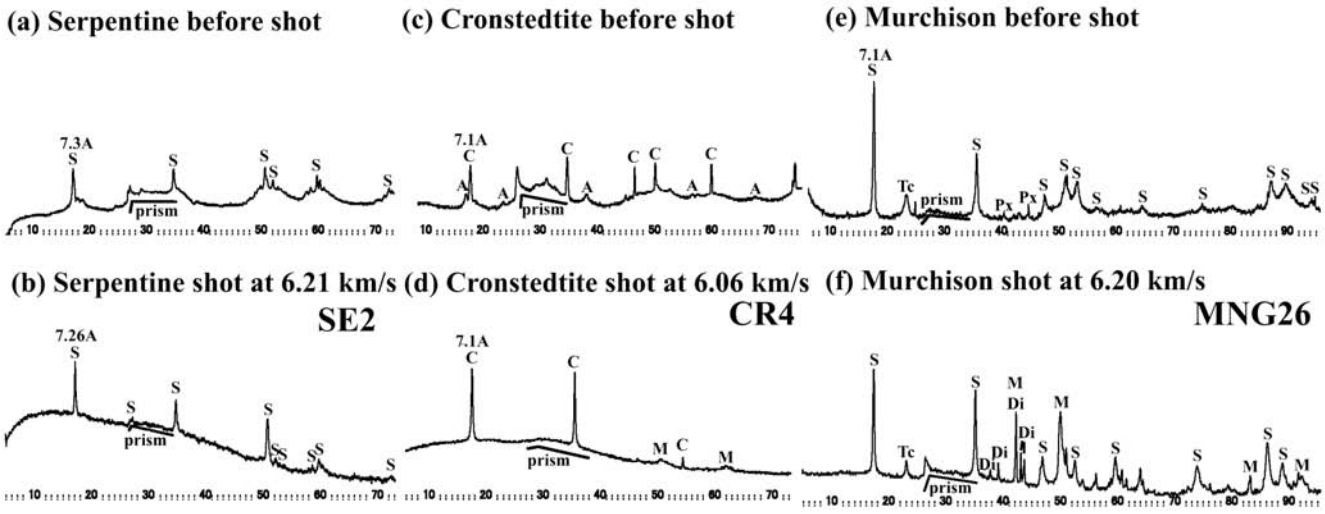

Fig. 1. Synchrotron radiation X-ray diffraction data of individual grains of serpentine, cronstedtite, and Murchison meteorite before and after hypervelocity capturing experiments. The abscissa axes of each X-ray charts are 2θ. Diffraction patterns of serpentine coincide with those of antigorite. No obvious change was detected in all the samples investigated except for cronstedtite shot at 6.06 km/s. S = serpentine, C = cronstedtite, Tc = tochilinite, M = magnetite, Di = diopside, A = akaganeite, prism = (02*l*) diffractions from serpentine.

samples. This result is also supported by TEM observation, which will be shown later. Another important observation is the presence of tochilinite in the captured Murchison powder MNG26 (Fig. 1h). The sharp diffraction peak of tochilinite (002) indicates that its structure was not modified during capture.

SEM Observation of Cross-Sections of the Captured Particles

Figure 2 displays backscattered electron (BSE) images of cross sections of the captured particles. The grains are <40 μm in the longest dimension (Fig. 2). When compared with serpentine and the other grains, captured cronstedtite and Murchison meteorite powder have rounded edges as indicated by the white arrows (Figs. 2b–d). At the opposite side of the rounded edge, vesicles are observed. Such large voids are absent in the serpentine grain (Fig. 2a). The captured cronstedtite is composed of relatively coarse (<5 μm across) grains and their interstices are filled with of fine grains and vesiculated glass (Fig. 2b), although the original size of each cronstedtite crystals was >100 μm in length. The texture of a captured Murchison particle and its EDS analysis suggest that the light gray prismatic to massive material is Fe-rich serpentine, that the interstitial dark gray materials are Fe- and Al-rich serpentine, and that the relatively dark material is Ca-rich pyroxene (Fig. 2c). It was probably a porphyritic pyroxene chondrule that experienced severe aqueous alteration because only Ca-rich pyroxene survives as anhydrous silicate. The particle in Fig. 2d is composed mainly of cronstedtite with a small amount of Ca-rich pyroxene, based on texture and EDS analysis. It also may have been a severely altered chondrule.

Table 1. Sample name and experimental conditions in this study and Okudaira et al. (2004).[a]

Sample name	Material	Shot speed (km/s)
#1	Antigorite	4.0[a]
SE2	Antigorite	6.21
#31	Cronstedtite	3.54[a]
CR4	Cronstedtite	6.06
MNG26	Murchison meteorite	6.20
MUR4	Murchison meteorite	6.18

[a]Antigorite is from Sambagawa, Gunma Prefecture, Japan; cronstedtite is from Salsigne mine, Aude, France.

TEM Observation of Ultrathin Sections of the Captured Particles

Serpentine

TEM observation of the ultrathin sections of serpentine revealed that melting and vesiculation occurred only at the very surface (Fig. 3). Low-magnification bright-field (BF) images of the surface demonstrate that the surface is composed of two layers: the outer vesiculated glass layer attached by silica aerogel and the inner partially decomposed serpentine layer. The outer and inner layers range from 0.5 to 1 μm thick and from 0.2 to 0.5 μm thick, respectively (Fig. 3a). Dark-field images of the layers show that both of them contain very fine-grained crystals <5 nm in diameter (Fig. 3b). In the partially decomposed serpentine layer, nanocrystals <2 nm across are dispersed in the partially decomposed serpentine (Fig. 3c). Although formation of nanocrystals occurred, the serpentine shows typical antigorite (*hk*0) diffraction spots with super lattice reflections along the a* direction displayed in the selected

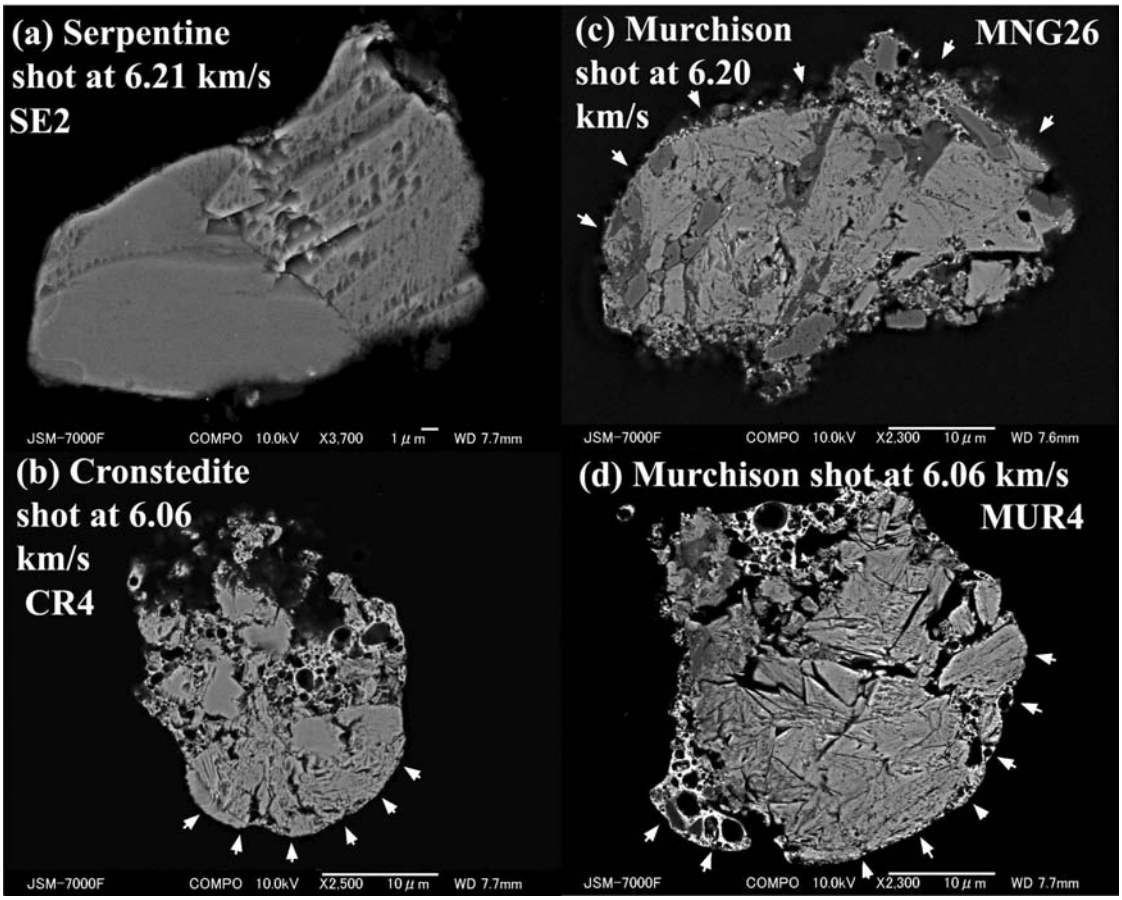

Fig. 2. Backscattered electron images of the individual grains of serpentine, cronstedtite, and Murchison meteorite. They correspond to the grains shown in Figs. 1b, 1d, 1e, and 1f. Obvious textural changes were found in the cronstedtite and Murchison meteorite samples shot at >6 km s^{-1}; melting and vesiculation is remarkable.

area electron diffraction (SAED) pattern in lower right inset. The upper right inset is the high-resolution image of the serpentine, with typical lattice fringes normal to the c-axis. In the SAED pattern, diffraction rings (indicated by white arrows) that originate from the nanocrystals overlap on the antigorite diffraction pattern. Their distances are 0.210 and 0.151 nm, which suggests wüstite, because its (200) and (220) are 0.214 and 0.151 nm, respectively, based on JCPDS. In the vesiculated glass, the included nanocrystals are about 5 nm across and larger than those in Fig. 3c, and also show the diffraction rings whose d-values are identical to those in Fig. 3c. These data suggest that the surface layers of the serpentine grain contain wüstite in spite of low iron content Mg/(Mg + Fe) atomic ratio >0.97 (Fig. 4).

EDS analysis of the vesiculated glass, partially decomposed serpentine, and unaltered serpentine are shown in Fig. 4. In this figure, EDS analyses of a serpentine grain shot at 4.0 km/s are also displayed for comparison. In the 4.0 km/s shot, the very surface of the sample, on which silica aerogel attached, showed no remarkable compositional change ("outer rim" in Fig. 4a). By contrast, vesiculated glass has variable compositions between serpentine and silica aerogel (Fig. 4b). This means that the glass was formed by melting and mixing of serpentine and aerogel. Partially decomposed serpentine has almost identical compositions to that of unaltered serpentine, which is common in the 4.0 km/s case.

Cronstedtite

TEM observation of cronstedtite grain captured at >6 km/s gives us a different picture of the interaction between a captured projectile and silica aerogel. Figure 5a is a low-magnification BF image of an ultrathin section of the captured particle shown in Figs. 1b and 2b on a lacy plastic supporting film. Because the cross section shown in Fig. 2b is the remainder after ultramicrotomy, the section in Fig. 5a is different in shape from Fig. 2b. In this figure, the upper left side of the thin section probably corresponds to the lower end of the cross section in Fig. 2b. This section has two "tails" that contain large (often >1 μm across) vesicles. These "tails" also contain small amounts of partially decomposed to unchanged cronstedtite. The side between the two "tails" is composed of a mixture of moderately to heavily vesiculated glass and partially decomposed to

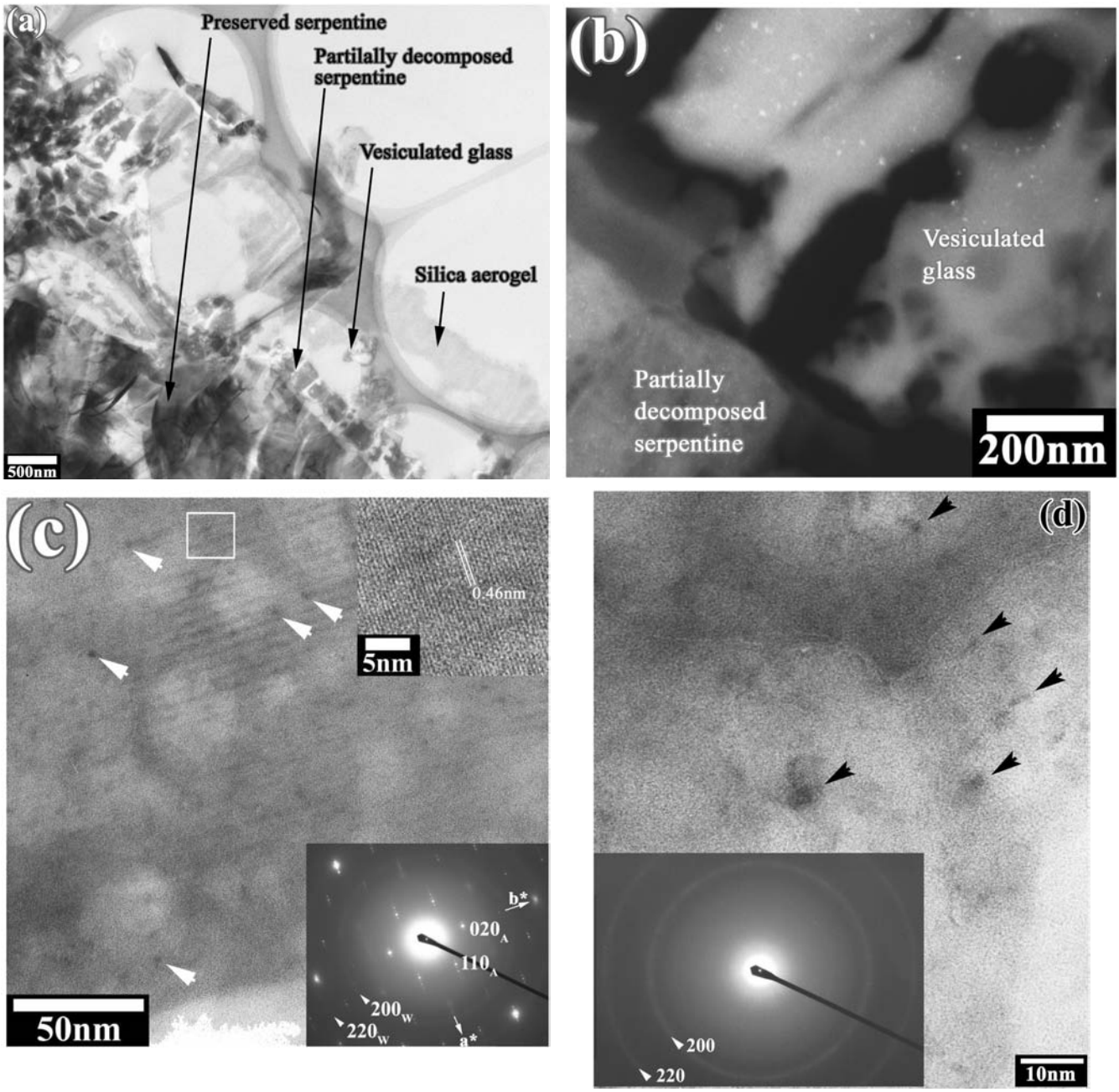

Fig. 3. TEM photomicrographs of ultrathin sections of a serpentine grain shot at 6.21 km s^{-1}. a) A low-magnification photograph of the cross section of the serpentine grain near its surface. The surface of the grain has a vesiculated glassy layer about 0.5 μm thick. It attaches the layer of partially decomposed antigorite with <0.3 μm thick. A light gray network shown in this photograph is the lacy formvar supporting film. b) A dark-field image of the boundary between the vesiculated glass and the partially decomposed serpentine. Fine-grained minerals were formed in both layers. c) Wüstite about 5 nm in size in the partially decomposed layer (from the selected electron diffraction [SAED] pattern, indicated by white arrows with indices of wüstite) imposed on the (hk0) SAED pattern of antigorite, which shows super lattice diffraction along a* of antigorite. The upper right inset shows (hk0) lattice fringes. d) TEM photomicrographs of ultrathin sections of a serpentine grain shot at 6.21 km s^{-1}. In the vesiculated glass, the SAED pattern (denoted by white arrows) indicates that the nanocrystals are wüstite.

unchanged cronstedtite. Compared with the side and the "tails," the upper left side of the grain has a thin (<0.3 μm thick) vesiculated glass coating. In the interior of the vesiculated surface layer, there are areas composed of a mixture of unaltered cronstedtite (1 to 3 μm across), vesiculated glass, and partially decomposed cronstedtite (Fig. 5b). It is interesting that vesicles in the interior tend to be larger than those at the upper left surface.

Figures 6a–c display higher magnification BF images of a 0.2 μm wide cronstedtite fragment and its surroundings. In

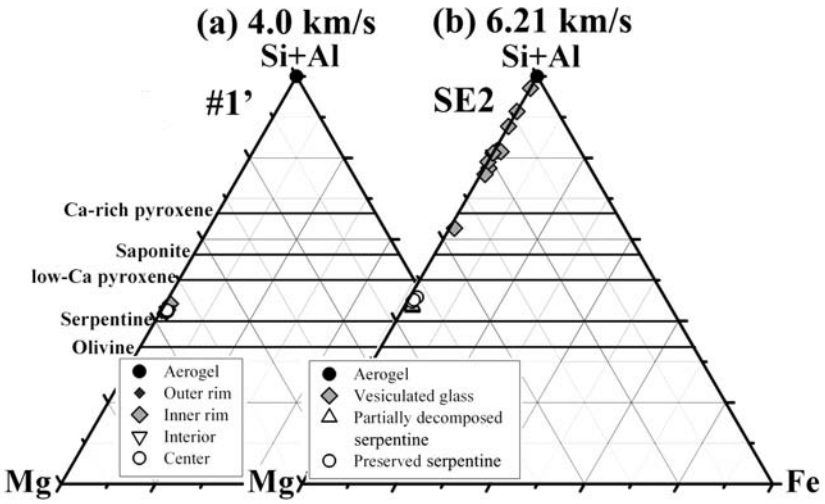

Fig. 4. The chemical compositions of materials in captured serpentine (antigorite) shot at 4.0 km s^{-1} and 6.21 km s^{-1}, obtained by analytical TEM (AEM). That there is a remarkable compositional variation in the vesiculated surface layer of the antigorite grain in the 6.21 km s^{-1} shot. The interior of the grain and that shot at 4.0 km s^{-1} have almost the same compositions as that of before shot.

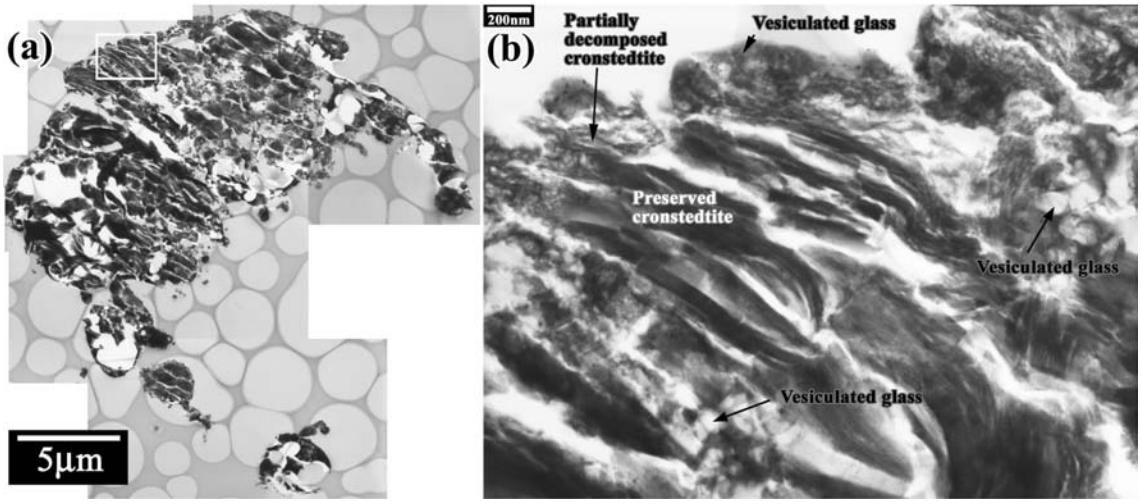

Fig. 5. A TEM photomicrograph of an ultrathin section of a cronstedtite grain shot at 6.06 km s^{-1}. a) Low-magnification TEM image of a whole cross section. While the upper left part of the section has a rounded smooth surface, the lower right portion of the section is vesiculated and heavier than the upper left portion with highly vesiculated "tails." Light gray network shown in this photograph is the lacy supporting plastic film. b) An enlarged image of the upper left surface of the sample indicated by a white rectangular in (a). In the surface (about 0.3 μm thick), vesiculated glass, partially decomposed cronstedtite, and unaltered cronstedtite are intermixed with one another, although the very surface (<0.2 μm thick) is covered by vesiculated glass layer.

the interior, the cronstedtite subgrain keeps (001) lattice fringes and clear (00l) diffraction row (Fig. 6b). At the boundary, crystalline cronstedtite becomes amorphous within 50 nm. In the transition area, (001) lattice fringes are dilute and the continuity of (001) lattice fringes is poor. Vesiculated glass contains abundant 20 nm size crystals (Fig. 6d). SAED pattern and high-resolution TEM image suggest that most of them are magnetite. This result is consistent with that obtained by SR-XRD (Fig. 1d).

In Fig. 7, EDS analyses of vesiculated glass, partially decomposed and unaltered cronstedtite are shown and those of cronstedtite from the shot at 3.54 km/s are also plotted for comparison. Compositions of vesiculated glass in the 6.06 km/s shot are closer to cronstedtite than those in the 3.54 km/s shot. It means that the vesiculated glass was a mixture of melted cronstedtite with minor melted silica aerogel. In both cases, partially decomposed cronstedtite (partially decomposed cronstedtite in Fig. 7b and cronstedtite, 150 nm from the rim in Fig. 7a) has chemical compositions almost identical to the unchanged cronstedtite.

Murchison CM2 chondrite

Overall textures of two captured Murchison particles from different shots are very similar to each other. They have

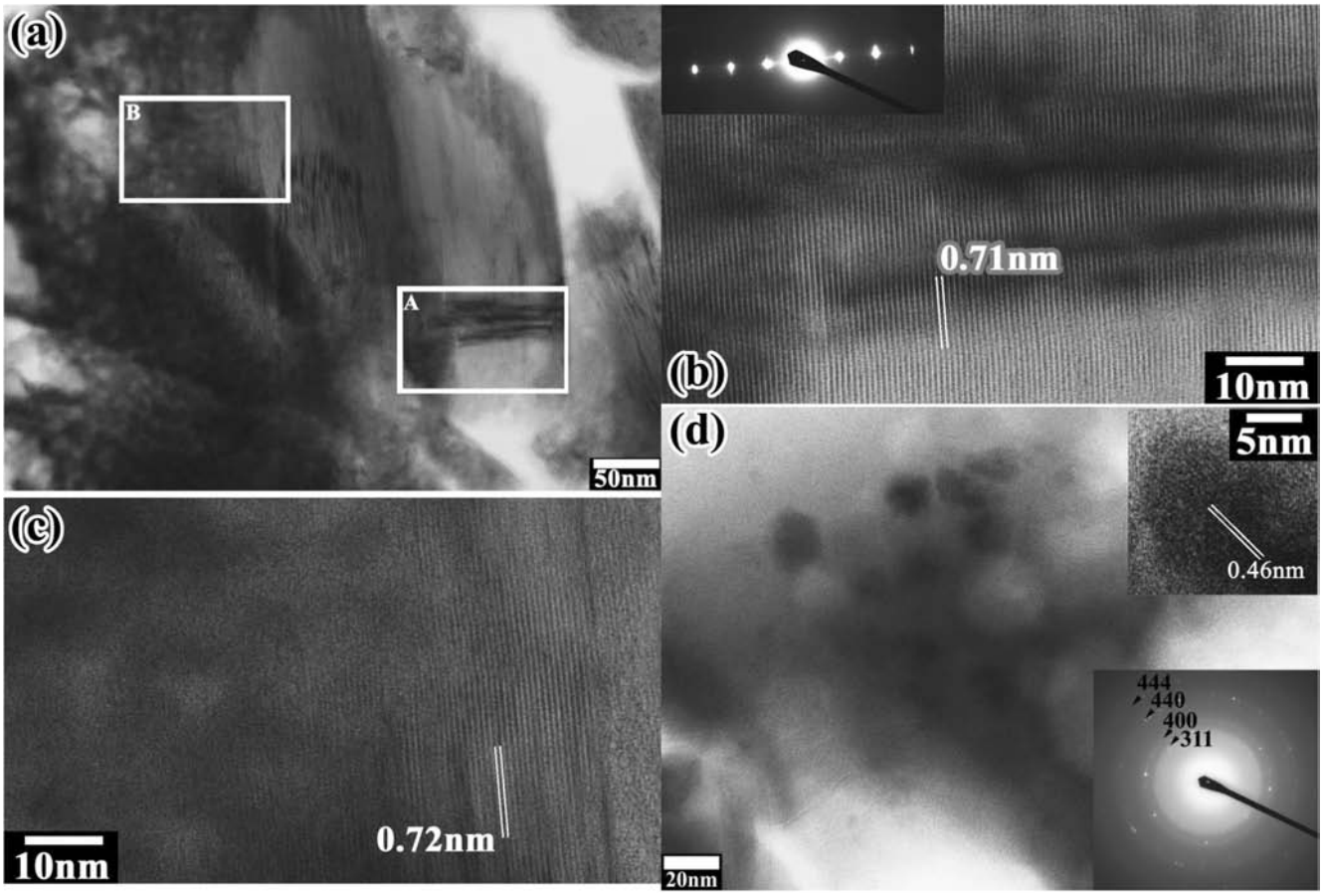

Fig. 6. a) This TEM image shows the relationship between a small (<0.1 μm in width) area of preserved cronstedtite and the surrounding materials formed by the decomposition of cronstedtite. b) An enlarged image of the center of the cronstedtite whose structure was unchanged during capture. c) At the boundary, (001) lattice fringes become vague and disappear within a distance of less than about 50 nm. d) In the vesiculated glass, 20 nm size magnetite nanocrystals are observed as indicated by the SAED pattern. The upper right inset shows a lattice image of a magnetite nanocrystal.

vesiculated surfaces, in which processed (from unchanged to melted) cronstedtite and Fe-rich serpentine are mixed together (Fig. 8a). The thickness of the vesiculated surface is typically <1 μm. The size of the vesicles in the surface area ranges from 0.2 to 0.3 μm across, which is comparable to those in the cronstedtite as shown in Fig. 5b. Destruction of the interior texture at a distance of >2 μm from the surface seems to be subtle (Fig. 8a). In both samples, the interiors are composed mainly of cronstedtite and Fe-rich serpentine with a small amount of Ca-rich pyroxene. A higher-magnification BF image of a fine-grained fragment of cronstedtite embedded in vesiculated glass is displayed in Fig. 8b. Vesiculated glass contains abundant nanocrystals <20 nm in diameter. Partially decomposed cronstedtite has fibrous morphology and contains fewer nanocrystals. The upper right inset of Fig. 8b is a high-resolution image of a fine-grained cronstedtite surrounded by amorphous material. It is composed of an intergrowth of cronstedtite (0.70 nm) and tochilinite (1.04 nm). The tochlinite is Fe-rich, because the (001) lattice fringes become obvious instead of the (002) lattice fringes when it has high Fe/(Fe + Mg) ratios (Nakamura and Nakamuta 1996).

Even in the vesiculated glass on the surface of the samples, Ca-rich pyroxene (augite) seems not to have been affected by melting of serpentines (Fig. 9a). No remarkable shock features such as dislocations, stacking faults, and mechanical twinning introduced during capture were recognized in Ca-rich pyroxene. In the SAED pattern of the pyroxene in the inset, diffraction spots are sharp and not distorted. In the vesiculated rim, the SAED pattern of the very fine-grained crystals suggests that the majority of them are magnetite. A high-resolution image of a nanocrystal shows 0.49 nm lattice fringes indicative of (111) magnetite lattice.

In the interior of the projectiles, hydrated minerals keep their structures and textures (Fig. 10). Figure 10a shows coexisting coarse cronstedtite and fine-grained Fe-rich serpentine, which is typical for heavily altered porphyritic chondrules in CM chondrites. The lower-left inset shows an enlarged image of the upper-left boxed

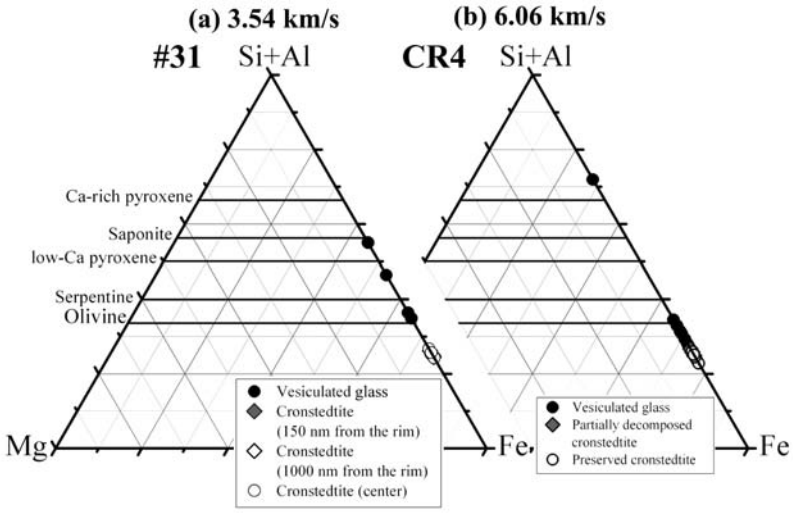

Fig. 7. An AEM analysis of the cronstedtite grain shot at 6.06 km s^{-1} shows that the vesiculated glass are plotted near cronstedtite except for one analysis, which contrasts the result of the 3.54 km s^{-1} shot. On the other hand, partially decomposed cronstedtite has chemical compositions similar to that of unaltered cronstedtite, which is common to those shot at 3.54 km s^{-1}.

area, which demonstrates that cronstedtite has sharp (001) lattice fringes. The upper-right inset enlarges the lower-right and boxed area. A high-resolution image of the fine-grained serpentine crystals shows that most of the (001) lattice fringes are curved, curled, cylindrical, and up to 30 nm thick, which is typical of (001). There is also serpentine with straight lattice fringes with <10 nm thick normal to (001). Tochilinite was observed as discrete crystals (Fig. 10b). It coexists with discrete crystals of cronstedtite. Tochilinite has sharp (002) lattice fringes, which are indicative of higher Mg concentration. The occurrence of these minerals indicates that they are type II PCP (Tomeoka and Buseck 1988).

EDS analyses of each phase in the two Murchison samples are shown in Fig. 11. In both samples, cronstedtite has a narrow compositional range, which is typical for cronstedtite in CM chondrites (Zolensky et al. 1993). However, fine-grained serpentine has different compositions between the two samples. In Fig. 11a, fine-grained serpentine is plotted around Fe/(Fe + Mg) = 0.5 and above the serpentine solid solution line due to high Al_2O_3 content (3.8 to 6.4 wt%). This is typical of fine-grained serpentine in chondrule mesostases. On the other hand, in Fig. 11b, most of the analyses are plotted between cronstedtite and serpentine with Fe/(Fe + Mg) ≈ 0.67. In both samples, partially decomposed serpentine and cronstedtite have almost identical compositions to those before the shot.

Vesiculated glass in Fig. 11a has variable chemical composition. Most of the analyses are plotted around the composition of cronstedtite, although some analyses deviate from cronstedtite to silica aerogel in Fig. 11a. These compositional data suggest that most of the vesiculated glass in captured Murchison originated from a mixture of abundant cronstedtite and a small amount of aerogel.

DISCUSSION

Size Reduction, Fracturing, Melting, and Vesiculation During Capture

It is not necessarily obvious that all the textural and mineralogical changes observed resulted from capture, because some of the textural changes could form during the hypervelocity launching. Therefore, we estimate the pressures loaded on the sample particles during launching. In our experiments, the acceleration rate at the instance of launch at 6 km s^{-1} is 1.8×10^7 m s^{-2}. The maximum pressure caused during hypervelocity launch is estimated at less than 4 MPa if we assume that each grain is composed of 150 μm size Murchison. Unconfined compression strength of Murchison meteorite is 50 MPa (Noguchi et al., unpublished data). Because tensile strength is about 1/10 of unconfined compression strength (Atkins and Mai 1988), what happens on the projectiles is fracturing at best. Therefore, we consider that the mineralogical changes observed in each sample were formed during capture.

Although the reduction of grain size during capture in aerogel has been already discussed by Okudaira et al. (2004), in which samples were shot at <4.5 km/s, the reduction of size is more conspicuous in this study. Grain sizes of captured projectile grains are much smaller than those of original ones. Captured particles of serpentine (antigorite), cronstedtite, and Murchison meteorite preserved only 0.1, 1.3, and 0.7–2.0% of their original volumes if we take a spherical approximation of the sample grains. These values are the lowest estimates because grain sizes of projectile powder were decreased by crushing in sabots at the instant of firing (Okudaira et al. 2003). Such size reduction of captured grains has been already recognized in a previous work using olivine,

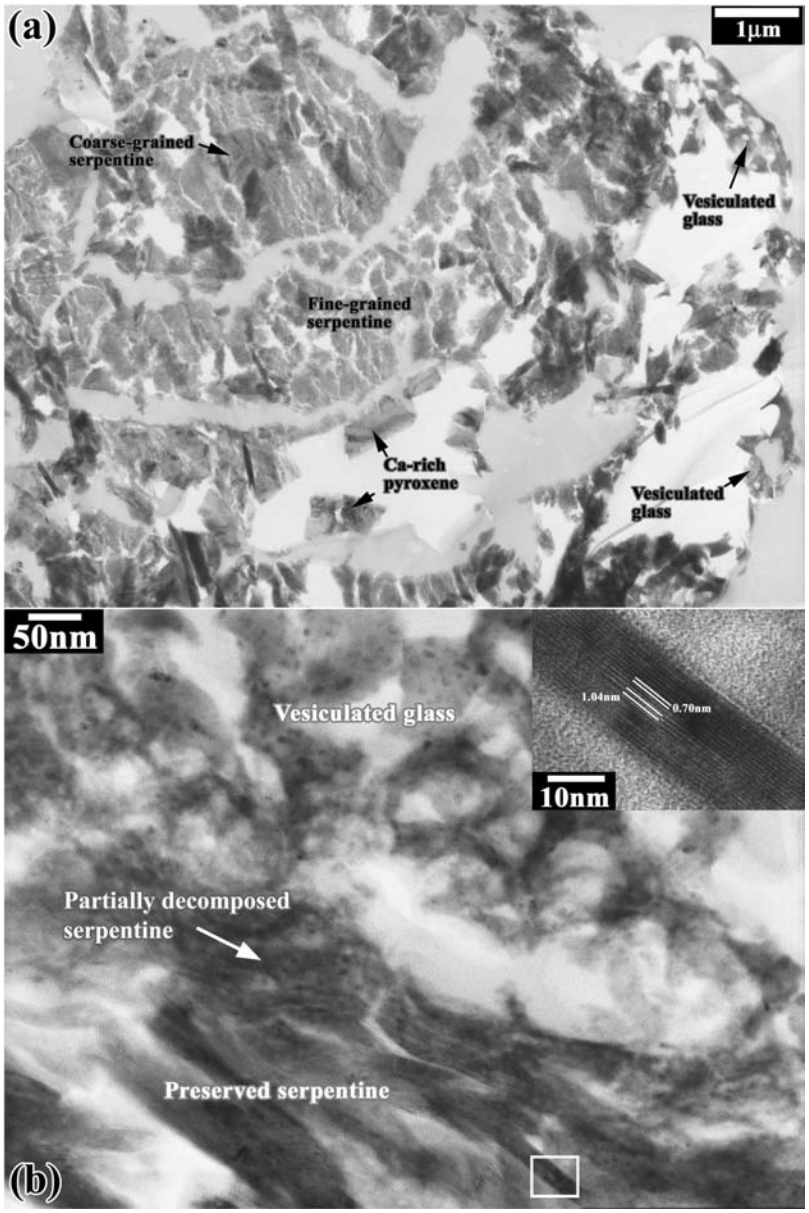

Fig. 8. TEM images of an ultrathin section of a fine-grained fragment of Murchison meteorite shot at 6.18 km s^{-1}. a) Low-magnification image of the section. Near the surface, vesiculated glass, decomposed serpentine, and preserved serpentine are intermixed with each other. The very surface is covered by the highly vesiculated glass. b) A higher magnification image of the intermixed layer. Upper right inset displays an enlarged view in the rectangular. Coexistence of lattice fringes with different spacing, 0.70 and 1.04 nm suggests that it is a mixture of cronstedtite and tochilinite.

pyroxene, and pyrrhotite shot at ~7 km s^{-1} (Barrett et al. 1992), although specific values of size reduction were not reported. These results clearly show that size reduction of captured grains is remarkable, irrespective of their mineral species, when projectiles are shot at >6 km s^{-1}.

There are three possible mechanisms to reduce grain size of projectile particles during capture in silica aerogel. The first is development of fracture at the "ram" face of the projectile grains and subsequent fragmentation of subgrains. The second possible mechanism is melting of the surface of the projectile grains due to frictional heating between the grains and silica aerogel and subsequent abrasion of the melted surface of the grains. The last mechanism is volatilization of the projectile grains due to intense frictional heating. As shown in Figs. 2b–d, it is obvious that fragmentation, melting, and vesiculation must have occurred during capture. Similar processing seems to have occurred during capture in the case of Murchison meteorite powder although the extents of these processes are lower than for cronstedtite. In reality, the first two mechanisms would have happened at the same time.

From the light flash at the impact of projectile grains,

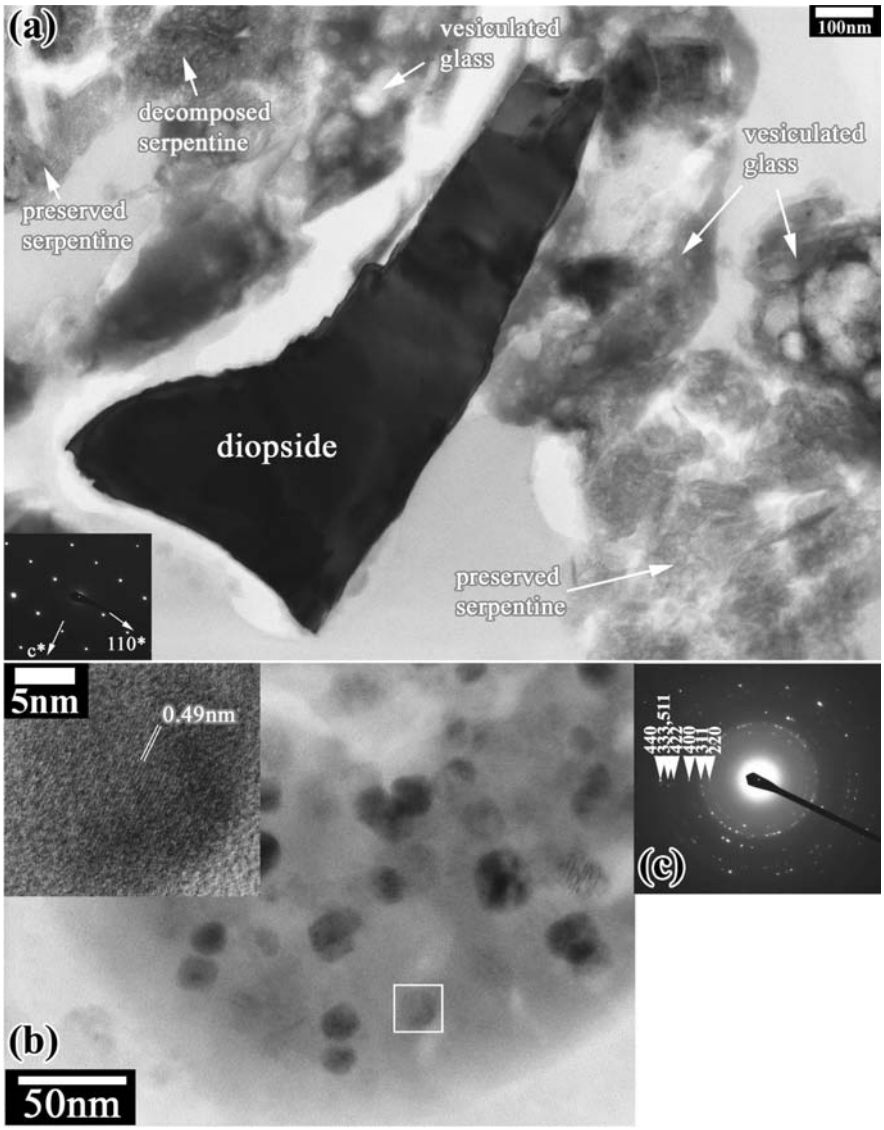

Fig. 9. TEM images of an ultrathin section of a fine-grained Murchison projectile shot at 6.20 km s^{-1}. a) Ca-rich pyroxene (augite) is not considerably affected on the surface. No obvious clues of deformation such as dislocation and mechanical twinning during capture were observed. b and c) High-resolution images of the nanocrystals and their SAED pattern revealed that the vesiculated glass contains abundant 20 nm size magnetite.

Okudaira et al. (2004) estimated 2000 ± 200 K for the maximum temperature during capture. We assessed the possibility of whether >98% volume loss was caused by evaporation of projectiles or not. Because hydrous minerals are preserved in the interior of projectiles, we assumed that dehydration and subsequent evaporation occurred only on the surface. We calculated the weight loss from 150 μm size sphere composed of material with solar system composition (near Fa_{50} olivine composition) by using the following values: evaporation rate of Fe, Si, and Mg at 1800 °C and 10^{-6} Torr; 1.26×10^{-4}, 1.99×10^{-5}, and 9.55×10^{-6} mole cm^{-2} s^{-1} (Wang et al. 2001), and capturing duration <1 μs (Brownlee et al. 2000). This crude estimation shows that about 1×10^{-8} of its weight is lost during capture. The decrease in volume is probably not far from this value (1×10^{-8}). Therefore, evaporation would have played a negligible role in reducing grain size if it had occurred, and even if the evaporation rate of our sample had been much higher than that of material with a solar abundance of elements. Stephan et al. (2006) performed hypervelocity capture experiments shot at 6 km s^{-1}. They used powdered Allende meteorite. They reported that silica aerogel is compositionally very clean in the vicinity of the tracks even by using highly sensitive TOF-SIMS. If evaporation of silicates had occurred during capture, elements typical for Allende matrix such as Mg and Fe would have been detected from outside the tracks. By considering these points, in the following, we will not discuss the effect of evaporation of silicates from projectile grains.

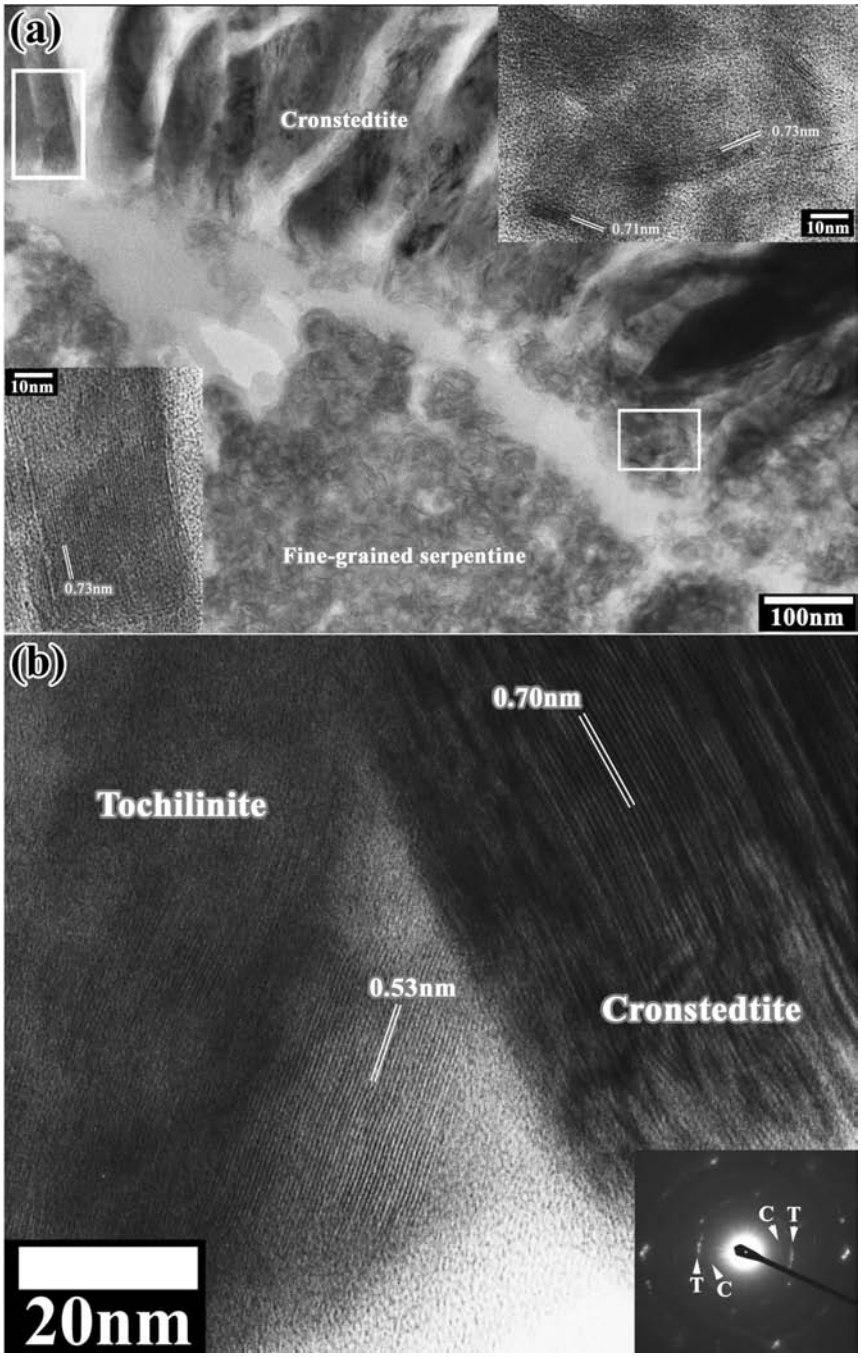

Fig. 10. The interior of the grain shown in Fig. 9. The interior texture of Murchison fragments shot at >6 km s^{-1} is preserved when compared with the near-surface area. a) Both coarse cronstedtite and fine-grained Fe-rich serpentine preserved their texture as a heavily altered chondrule. High-resolution images of preserved minerals show that sharp lattice fringes are observed even in the fine-grained serpentine (upper-right inset). b) Coexistence of cronstedtite and tochilinite as individual mineral grains. The occurrence suggests that it is type II PCP (poorly characterized phase). Abbreviations are C (cronstedtite) and T (tochilinite).

The degrees of melting and vesiculation of the projectiles are more conspicuous in both cronstedtite and Murchison meteorite than for serpentine. The decomposition temperature of cronstedtite was previously measured as 470 °C by differential thermal analysis (Caillère and Hénin 1957). The decomposition temperature of Fe-rich serpentine in Murchison was estimated as 600–660 and 500–600 °C by TEM and SR-XRD, respectively (Akai 1992; Nozaki et al. 2006). That of antigorite is 650–700 °C (e.g., Brindley and Bussmann 1957). Therefore, the difference in melting and vesiculation is probably due to the difference of decomposition temperatures among these materials. The

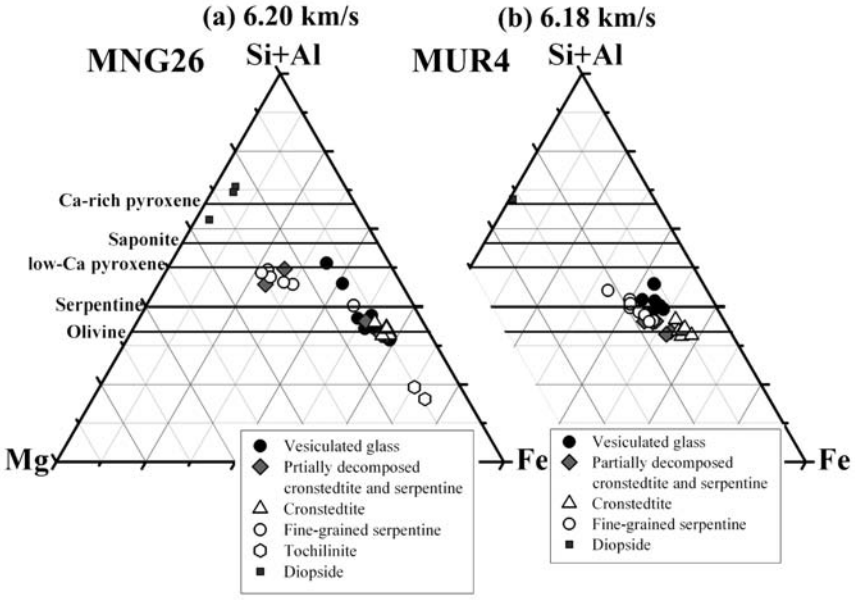

Fig. 11. Chemical compositions of two Murchison fragments obtained by AEM. Vesiculated glass has compositions between cronstedtite and silica aerogel although most are plotted near cronstedtite. On the other hand, decomposed serpentine are plotted in almost the same areas as cronstedtite and fine-grained, Fe-rich serpentine. Due to the large electron beam diameter (200–500 nm), "tochilinite" in (a) has a chemical composition of a mixture of tochilinite and coexisting cronstedtite.

melted surface layer of antigorite is a mixture of silica aerogel and antigorite. On the contrary, those of cronstedtite and Murchison meteorite were made almost wholly of themselves (Figs. 4, 7, and 11).

We observed diopsidic Ca-rich pyroxene in the melted and vesiculated layer on the surface of Murchison meteorite powder (Fig. 9). Even using TEM, we could not acquire obvious clues for melting of diopside. Therefore, the temperature on the surface of projectile did not exceed the melting temperature of diopside (1391 °C) (Bowen 1915). Toppani et al. (2001) stated that remarkable melting occurred in micrometeorites when the micrometeorites were heated above 1200 °C. Their SEM images show that slight changes occurred when the samples were heated at 1000 °C. Nozaki et al. (2006) recognized that the onset of melting and vesiculation started at 1000 °C on the TEM scale. If we use these values, the surfaces of the Murchison powder are thought to have experienced temperatures above 1000 and below 1390 °C.

Tsou (1995) presented a schematic illustration of a captured projectile grain that has a similar shape to those of captured cronstedtite and Murchison powder. In Fig. 4 of Tsou (1995), the "ram" face of the captured projectile was rounded. If this morphological feature can be applicable to this study, the rounded sides of the cross sections of CR4, MNG26, and MUR4 are thought to be the "ram" faces (Figs. 2b–d). Because the thickness of the amorphous layer at the rounded side of the captured grains is smaller (100 nm) than the other sides (<200 nm), it is suggested that melted material was efficiently removed from the "ram" faces. Figures 2b–d also show that the size of vesicles in the glass tend to be larger at the "wake" faces of the captured particles. The increase of vesicle sizes may be related to the decrease of pressure toward the "wake" side.

Heating during Capture Estimated from Decomposition and Melting of Cronstedtite

Although both cronstedtite and Murchison meteorite powder captured at >6 km s^{-1} were fractured into some subgrains and melting, and vesiculation occurred among subgrains, the surfaces of the entire grains have thin (0.2–1 μm) melted and vesiculated layers (Figs. 2, 5, 6, 8, and 9; Table 2). There are areas made of partially decomposed to totally amorphous cronstedtite or Fe-rich serpentine just inside the surface layers. One of the Murchison samples, MUR4, is composed mainly of cronstedtite as phyllosilicates (Fig. 11). TEM observation of surfaces of cronstedtite sample CR4 and Murchison powder MUR4 exemplifies that they have melted and vesiculated surfaces about 0.1 to 0.3 μm thick and amorphous to partially decomposed layers 0.1 to 0.2 μm thick except for "wake" faces and "tails." Because decomposition of cronstedtite starts at 470 °C (Caillère and Hénin 1957) and the amorphous to partially decomposed layers do not show conspicuous vesiculation, it is thought that the amorphous layers experienced about 470 to 1000 °C. In the interior of another Murchison powder MNG26, tochilinite was intact. Because the decomposition temperature of tochilinite is about 300 °C, there must have been a steep thermal gradient near the surfaces of the captured projectiles;

Table 2. Modification of minerals on the surface of captured samples.

Mineral	Sample	Shot speed (km/s)	Modification on the surface	Modification near the surface (<1–2 μm from the surface)	Decomposition temperature
Antigorite	#1	4.0	Partially decomposed, not vesiculated	Not changed	650–700 °C[a]
Antigorite	SE2	6.21	Vesiculation	Partially decomposed to amorphous state	
Cronstedtite	#31	3.54	Vesiculation	Partially decomposed to amorphous state	470 °C[b]
Cronstedtite	CR4	6.06	Heavy vesiculation	From partially decomposed to totally amorphous, intermixed with melted and heavily vesiculated material	
Cronstedtite	MUR4, MNG26	6.18, 6.20	Heavy vesiculation	From partially decomposed to totally amorphous, intermixed with melted and heavily vesiculated material	
Fe-rich serpentine	MUR4	6.18	Heavy vesiculation	From partially decomposed to totally amorphous, intermixed with melted and heavily vesiculated material	500–600 °C[c, d]
Tochilinite	MNG26	6.20	Not found	Not changed	300 °C[c, d]
Ca-rich pyroxene	MUR4, MNG26	6.18, 6.20	Not changed	Not changed	1391 °C (melting temperature of pure diopside)[e]

[a]Brindley and Zussmann (1957).
[b]Caillère and Hénin (1957).
[c]Fuchs et al. (1973).
[d]Nozaki et al. (2006).
[e]Bowen (1915).

about 2500 °C/μm, and the interior of the captured grains have not experienced >300 °C during capture (Fuchs et al. 1973; Nozaki et al. 2006).

We performed a rough calculation of heating duration to reproduce the estimated thermal gradient near the surfaces of the projectiles using the following equation:

$$\frac{\rho c_v}{K}\frac{\partial v}{\partial t} = \frac{\partial^2 v}{\partial \xi^2} \quad (1)$$

where v is temperature, ξ is time, ρ is density, c_v is heat capacity, and K is thermal conductivity.

To calculate this thermal conduction in the projectiles, the density ρ, heat capacity c_v, and thermal conductivity K of each mineral are needed. We used ρ, c_p, and K of antigorite because of the lack of c_v and K for cronstedtite (Berman and Brown 1985; Horai 1971). We used heat capacity c_p instead of c_v because c_p only differs in a few percent from c_v (see text books of statistical physics such as Lifshitz and Landau), and because there are data for c_p for many minerals. We could not observe recrystallized olivine and pyroxene in both of the partially decomposed to amorphous area and the melted surface. We calculated the heat capacity of antigorite at 1000 °C based on the formula of Berman and Brown (1985). The calculated temperature diffusivity of antigorite is 5.5×10^{-8} m^2 s^{-1}, which is <1/20 of the calculated value of olivine. The other anhydrous minerals have similar values of temperature diffusivity to that of olivine (Clauser and Huenges 1995). Figure 12 is a result of a simple calculation when a projectile at the room temperature is heated to 1300 °C giving the thermal gradient within the grain during heating. This figure indicates that thermal gradients as steep as those estimated by TEM observation are accomplished only when they are heated for a very short time (<1.8 μs in this figure). If the temperature diffusivity of cronstedtite is higher than that of antigorite, shorter heating duration is appropriate. In this study, heating duration was probably from about 0.1 (~1/20 of 1.8 μs) to 1.8 μs. Brownlee et al. (2000) found that the captured grain will come to a dead stop within 1 μs. Although this crude calculation does not consider the effect of melting as performed by Flynn (1995), it seems to be consistent with his statement. In reality, removal of hot materials from the surface of a projectile by abrasion and endothermic dehydration reaction of cronstedtite on the surface also play important roles to reduce the increase of temperature and make thermal gradient steeper just within the surface.

Barrett et al. (1992) reported that olivine, pyrrhotite, and calcite shot at 5–7 km s^{-1} were highly brecciated, locally volatilized, melted, and welded together with fractured and melted aerogel. In their experiments, pyrrhotite experienced extensive modification including reduction to Fe metal, and no calcite grain was recovered from the top ends of the tracks in aerogel. Pyrrhotite decomposes by frictional heating at about 700 °C if pyrometamorphic reaction of pyrrhotite in IDPs is applicable (Rietmeijer 2004) and decarbonation of calcite occurs under a vacuum condition at about 750 °C (Engler 1988). These values are not so low when compared with cronstedtite and antigorite. It is likely that higher temperature diffusivities of these minerals are responsible for the poor preservation of residual material. In other words, preservation of original mineralogy in the residual material depends on the presence of abundant materials that inhibit temperature rise in the interior during capture. A euhedral pyrrhotite crystal in a micrometeoroid captured by silica

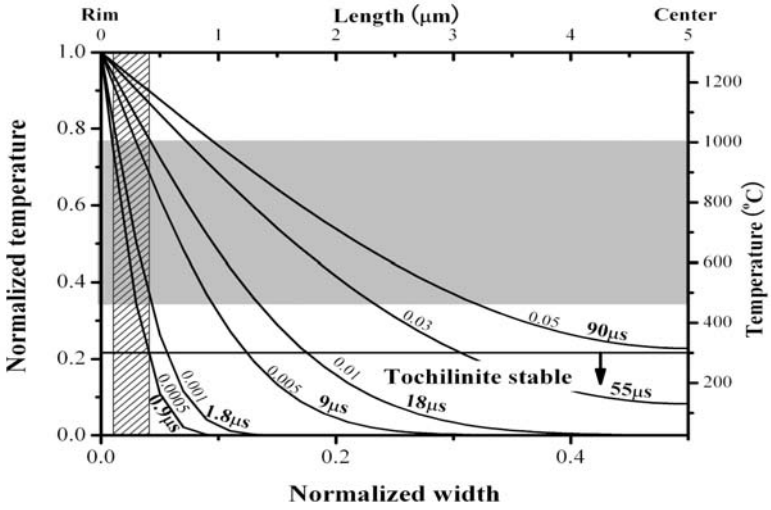

Fig. 12. Calculation of thermal gradient in a serpentine projectile grain during capture. To accomplish steep thermal gradient observed in this study, quite short heating (<1 μm) is needed. This graph also shows that temperature increase in the interior of the projectile is low enough to preserve materials that are susceptible to breakdown.

aerogel collectors aboard Mir is reported (Hörz et al. 2000). In this particle, pyrrhotite is embedded in poorly crystallized silicate material as well as olivine, chromite, and hercynite. Poorly crystallized silicate material may also serve as material that inhibits temperature rise in its interior.

Implication for Returned Samples of the Stardust Mission

The Stardust mission has returned cometary dust to the Earth from comet P81/Wild-2 (e.g., Zolensky et al. 2006). The relative velocity of cometary dust during the encounter of the Stardust spacecraft with the comet was 6.1 km s^{-1}, which is similar to experimental conditions in this study. Our study suggests that preservation of original texture and mineralogy of captured particles depends on decomposition temperature, temperature diffusivity, and disruptive strength of each mineral. Another important factor for the preservation of sample is the effect of endothermic phase transition (Flynn 1995). It is believed that organic materials showing endothermic phase transitions connect and enclose the other components in cometary dust. Because serpentine group minerals that are important for reducing the increase of temperature in the interior are probably absent or very minor in cometary dust, the abundance of carbonaceous material is key to the preservation of primary features of cometary dust. Our study suggests that the interior (1–2 μm from the surface) of residual grains would not have experienced remarkable heating if they contain abundant hydrated minerals that inhibit increase in temperature. Therefore, the interior of the captured grains larger than 4 μm containing abundant carbonaceous material as an inhibitor of temperature rise or much larger grains composed of a coherent aggregate of anhydrous minerals are suitable for the investigation of primary features of cometary dust.

CONCLUSIONS

We performed a detailed mineralogical study of serpentine, cronstedtite, and Murchison CM2 meteorite powder that was captured in silica aerogel. The samples were shot at >6 km s^{-1} similar to Stardust's flyby speed near comet Wild-2. The average grain sizes of captured particles are 10–30 μm, reduced to 0.1–0.2 of their original grain sizes. SR-XRD of each grain shows that the majority of the bulk materials kept their original mineralogy. SR-XRD and TEM investigations clearly showed that tochilinite (whose decomposition temperature is 300 °C) in the interior of the captured grains is intact. However, TEM study of these grains revealed that all samples experienced melting and vesiculation on the surface. Cronstedtite and Murchison meteorite powder especially show remarkable fracturing, disaggregation, melting, and vesiculation. It is clear that the extent of modification depends on decomposition temperatures of constituents in the grains. Steep thermal gradient (about 2500 °C/μm) near the surface of the grains was estimated from TEM observation of near-surface microstructure of cronstedtite and Murchison powder. Our data suggest that captured grains that contain abundant carbonaceous material larger than 4 μm or much larger grains composed of a coherent aggregate of anhydrous minerals are suitable for the study of primary features of cometary dust that will be returned by the Stardust mission.

Acknowledgments–We thank Dr. M. Tanaka and Mr. T. Mori for supporting synchrotron radiation X-ray diffraction experiments at the High-Energy Physics Research Organization. We also appreciate Mr. T. Yanagihara for supporting FE-SEM observation at JEOL, Ltd. Dr. M. E. Zolensky and an anonymous reviewer are appreciated for

their constructive comments. This manuscript was revised during the stay of Noguchi at the University of Muenster. This work is supported by the grants from the Ministry of Sports, Science, and Culture (to Noguchi: #13440158 and 17340157) and by the grant of the Space Forum (to Yano).

Editorial Handling—Dr. Hiroko Nagahara

REFERENCES

Akai J. 1992. T-T-T diagram of serpentine and cronstedtite, and estimation of metamorphic heating degree of Antarctic carbonaceous chondrites. *Proceedings of the NIPR Symposium on Antarctic Meteorites* 5:120–135.

Atkins A. G., and Mai Y.-W. 1985. *Elastic and plastic fracture: Metals, polymers, ceramics, composites, biological materials.* Ellis Horwood Series in Engineering Science. Chichester: Ellis Horwood, Ltd. 817 p.

Barrett R. A., Zolensky M. E., Hörz F., Lindstrom D. J., and Gibson E. K. 1992. Suitability of silica aerogel as a capture medium for interplanetary dust. Proceedings, 22nd Lunar and Planetary Science Conference. pp. 203–212.

Berman R. G. and Brown T. H. 1985. Heat capacity of minerals in the system Na_2O-K_2O-CaO-MgO-FeO-Fe_2O_3-Al_2O_3-SiO_2-TiO_2-H_2O-CO_2: Representation, estimation, and high temperature extrapolation. *Contributions to Mineralogy and Petrology* 89: 168–183.

Bowen N. L. 1915. The crystallization of haplobasaltic, haplodioritic, and related magmas. *American Journal of Science* 40:161–185.

Brindley G. W. and Zussmann J. Z. 1957. A structural study of the thermal transformation of serpentine minerals to forsterite. *American Mineralogist* 42:461–474.

Brownlee D. E., Tsou P., Clark B., Hanner M. S., Hörz F., Kissel J., McDonnell J. A. M., Newburn R. L., Sandford S., Sekanina Z., Tuzzolino A. J., and Zolensky M. E. 2000. Stardust: A comet sample return mission (abstract). *Meteoritics & Planetary Science* 35:A35.

Brownlee D. E., Anderson J. D., Atkins K., Bhaskaran S., Cheuvront R. A., Clark B. C., Duxbury T. C., Economou T., Hanner M. S., Hörz F., Kissel J., McDonnell J. A. M., Green S., Newburn R. L., Perkins D. E., Price S., Ryan R. E., Sandford S. A., Sekanina Z., Tsou P., Tuzzorio A. J., Villinga J. M., Williams K. E., and Zolensky M. E. 2004. Stardust—A successful encounter with the remarkable comet Wild-2 (abstract #1981). 35th Lunar and Planetary Science Conference. CD-ROM.

Burchell M. J., Thomson R., and Yano H. 1999. Capture of hypervelocity particles in aerogel in ground laboratory and low Earth orbit. *Planetary and Space Science* 36:189–204.

Burchell M. J., Graham G., and Kearsley A. 2006 Cosmic dust collection in aerogel. *Annual Review of Earth and Planetary Science* 34:385–418.

Caillère S. and Hénin S. 1957. The chlorite and serpentine minerals. In *The differential thermal investigation of clays*, edited by MacKenzie R. C. London: UK Mineralogical Society. pp. 207–230.

Clauser C. and Huenges E. 1995. Thermal conductivity of rocks and minerals. In *Rock physics and phase relations—A handbook of physical constants*, edited by Ahrens T. J. Washington, D.C.: American Geophysical Union. pp. 105–126.

Engler P., Santana M. W., Mittleman M. L., and Balazs D. 1988. Non-isothermal in situ XRD analysis of dolomite decomposition. *The Rigaku Journal* 5:3–8.

Flynn G. J. 1995. Thermal gradient in interplanetary dust particles: The effect of an endothermic phase transition (abstract). 26th Lunar and Planetary Science Conference. pp. 405–406.

Fuchs L. H., Olsen E., and Jensen K. J. 1973. Mineralogy, mineral chemistry, and compositions of the Murchison (C2) meteorite. *Smithsonian Contributions to Earth Science* 10:1–39.

Horai K. 1971. Thermal conductivity of rock-forming minerals. *Journal of Geophysical Research* 76:1278–1308.

Hörz F., Zolensky M. E., Bernhard R. P., See T. H., and Warren J. L. 2000. Impact features and projectile residues in aerogel exposed on Mir. *Icarus* 147:559–579.

Hunt A. J., Jantzen C. A., and Cao W. 1991. Aerogel: A high-performance insulating material at 0.1 bar. In *Insulation materials: Testing and applications II*, edited by Graves R. S. and Wysocki D. C. Philadelphia: American Society for Testing and Materials. pp. 455–463.

Lifshitz E. M. and Landau L. D. 1980. *Statistical physics*. Oxford: Butterworth-Heinemann. 544 p.

Nakamura T. and Nakamuta Y. 1996. X-ray study of PCP from the Murchison CM carbonaceous chondrite. *Proceedings of the NIPR Symposium on Antarctic Meteorites* no. 9. pp. 37–50.

Nakamura T., Noguchi T., Yada T., Nakamuta Y., and Takaoka N. 2001. Bulk mineralogy of individual micrometeorites determined by X-ray diffraction analysis and transmission electron microscopy. *Geochimica et Cosmochimica Acta* 65: 4385–4397.

Neish M. J., Kitazawa Y., Noguchi T., Inoue T., Imagawa K., Goka T., and Ochi Y. 2005. Passive measurement of dust particles on the ISS using MPAC: Experiment summary, particle fluxes, and chemical analysis. Proceedings, Fourth European Conference on Space Debris. pp. 221–226.

Nozaki W., Nakamura T., and Noguchi T. 2006. Bulk mineralogical changes of hydrous micrometeorites during low-temperature heating in the upper atmosphere. *Meteoritics & Planetary Science* 41:1095–1114.

Okudaira K., Noguchi T., Nakamura T., Burchell M. J., Cole M., and Yano H. 2003. Assessment of analog particle capturing by aerogel at the flyby speed of Stardust. (abstract #6024). Workshop on Cometary Dust in Astrophysics. CD-ROM.

Okudaira K., Noguchi T., Nakamura T., Sugita S., Sekine Y., and Yano H. 2004. Evaluation of mineralogical alteration of micrometeoroid analog materials captured in aerogel. *Advances in Space Research* 34:2299–2304.

Okudaira K., Yano H., Noguchi T., Nakamura T., Burchell M. J., and Cole M. J. 2005. Are they really intact? Evaluation of captured micrometeoroid analogs by aerogel at the flyby speed of Stardust (abstract #1832). 36th Lunar and Planetary Science Conference. CD-ROM.

Rietmeijer F. J. M. 2004. Dynamic pyrometamorphism during atmospheric entry of large (~10 micron) pyrrhotite fragments from cluster IDPs. *Meteoritics & Planetary Science* 39:1869–1887.

Rietmeijer F. J. M. 2004. Interplanetary dust and carbonaceous meteorites: Constraints on porosity, mineralogy, and chemistry of meteors from rubble-pile planetesimals. *Earth, Moon, and Planets* 95:321–338.

Stephan T., Butterworth A. L., Hörz F., Snead C. J., and Westphal A. J. 2006. TOF-SIMS analysis of Allende projectiles shot into silica aerogel. *Meteoritics & Planetary Science* 41:211–216.

Tomeoka K. and Buseck P. R. 1988. Indicators of aqueous alteration in CM carbonaceous chondrites: Microtextures of a layered mineral containing Fe, S, O and Ni. *Geochimica et Cosmochimica Acta* 49:2149–2163.

Toppani A., Libourel G., Engrand C., and Maurette M. 2001. Experimental simulation of atmospheric entry of micrometeorites. *Meteoritics & Planetary Science* 36:1377–1396.

Tsou P. 1995. Silica aerogel captures cosmic dust intact. *Journal of Non-Crystalline Solids* 186:415–427.

Wang J., Davis A. M., Clayton R. N., Mayeda T. K., and Hashimoto A. 2001. Chemical and isotopic fractionation during the evaporation of the FeO-MgO-SiO_2-CaO-Al_2O_3-TiO_2 rare earth element melt system. *Geochimica et Cosmochimica Acta* 65:479–494.

Zolensky E. M., Zega T. J., Yano H., Wirick S., Westphal A. J., Weisberg M. K., Weber I., Warren J. L., Velbel M. A., Tsuchiyama A., Tsou P., Toppani A., Tomioka N., Tomeoka K., Teslich N., Taheri M., Susini J., Stroud R., Stephan T., Stadermann F. J., Snead C. J., Simon S. B., Simionovici A., See T. H., Robert F., Rietmeijer F. J. M., Rao W., Perronnet M. C., Papanastassiou D. A., Okudaira K., Ohsumi K., Ohnishi I., Nakamura-Messenger K., Nakamura T., Mostefaoui S., Mikouchi T., Meibom A., Matrajt G., Marcus M. A., Leroux H., Lemelle L., Le L., Lanzirotti A., Langenhorst F., Krot A. N., Keller L. P., Kearsley A. T., Joswiak D., Jacob D., Ishii H., Harvey R., Hagiya K., Grossman L., Grossman J. N., Graham G. A., Gounelle M., Gillet P., Genge M. J., Flynn G., Ferroir T., Fallon S., Ebel D. S., Dai Z. R., Cordier P., Clark B., Chi M., Butterworth A. L., Brownlee D. E., Bridges J. C., Brennan S., Brearley A., Bradley J. P., Bleuet P., Bland P. A., and Bastien R. 2006. Mineralogy and petrology of comet Wild-2 nucleus samples. *Science* 314:1735–1739.